Journal of Materials Chemistry C

COMMUNICATION

View Article Online
View Journal | View Issue

Cite this: J. Mater. Chem. C, 2016, 4, 9656

Received 20th May 2016,
Accepted 13th September 2016

DOI: 10.1039/c6tc02089e

www.rsc.org/MaterialsC

A fused thieno[3,2-*b*]thiophene-dithiophene based donor molecule for organic photovoltaics: a structural comparative study with indacenodithiophene†

Yuichiro Abe,[abc] Hairong Li,[a] Jun Yin,[d] Cesare Soci,[d] Andrew C. Grimsdale[a] and Yeng Ming Lam*[a]

A novel donor material, di(HTh2BT)DTCTT, having a dithienocyclopentathieno[3,2-*b*]thiophene (DTCTT) core, was synthesized and used as the molecular donor in a small molecular organic photovoltaic device (sm-OPV). DTCTT has a molecular structure similar to that of indacenodithiophene (IDT) but with a central thienothiophene instead of a benzene, and the effect of the more extended conjugation of the theinothiophene on its optical, thermal and photovoltaic properties was systematically investigated. Di(HTh2BT)DTCTT showed red-shifted absorption (up to 800 nm), a higher HOMO level and greater crystallinity than its IDT analogue. The DTCTT based sm-OPV devices were fabricated by spin-coating a blend solution with $PC_{71}BM$, and showed an encouraging PCE of 2.8% with J_{sc} of −9.3 mA cm^{-2}, V_{oc} of 0.73 V and FF of 0.42. This is the first report of a DTCTT-based molecular donor for sm-OPV and it can be seen that this compound has greater potential for achieving high efficiencies compared with its IDT analogue. The structural and morphological analyses indicated that further improvement may be possible by increasing the crystallinity of the blend film.

Introduction

Indacenodithiophene (IDT) has been attracting considerable attention as a building block in organic semiconductors. Its coplanarity and extended conjugation are beneficial for charge transport, making it a good polymeric semiconductor as polymers containing it have shown to have mobilities of over 1 cm^2 V^{-1} s^{-1} in organic field effect transistors (OFET).[1–3] In addition, it has been coupled with a variety of acceptor units to form donor–acceptor (D–A) type polymers and these have shown to have potential for application in polymer solar cells (PSC).[4–6] One such successful D–A polymer is IDT coupled with a benzo[2,1,3]thiadiazole (BT) unit which, when blended with a fullerene acceptor, produced a very promising power conversion efficiency (PCE) of 6.4%.[7] Recently, IDT has been incorporated into D_1–A–D_2–A–D_1 type molecules and has been tested in small molecular photovoltaic devices (sm-OPV)[8–10] with promising results.[11–13] In particular, a device fabricated with a molecular donor containing units of IDT substituted with solubilizing alkyl side chains on its sp^3 carbons and difluorobenzo-[2,1,3]thiadiazole (2FBT) showed a PCE of 8.1%, which is among the highest values yet reported for a sm-OPV.[14] Furthermore, IDT has also been coupled with electron deficient units in an attempt to make efficient n-type semiconducting materials, which might be good candidates to replace fullerene acceptors. Some of them have been mixed with polymer donors and PCEs of nearly 10% have been achieved.[15–18]

These results showed that the IDT structure is a promising building block for the further development of OPV materials, and thus utilizing the family of other fused ladder-type arenes[19,20] can potentially be the direction for future research in this area. However, it remains to be seen how the structure influences OPV device performance. Much attention has been paid to the relationship between the solid-state intermolecular interaction, nano-structured morphology and optoelectronic properties of organic materials. Recent attempts at the development of materials for sm-OPV, demonstrated that their solid-state properties vary in a complex fashion with a variety of structural factors such as the presence of hetero atoms,[21,22] the nature, position and number of side chains,[23,24] and structure of the backbone.[13,25,26] Systematic investigation is necessary to elucidate the solid-state structure/properties relationships needed for the rational design of an efficient OPV material.[9] Molecular materials are good candidates for this purpose as they have a defined structure unlike polymer materials which have structural uncertainty in important parameters such as the degree of polymerization, the molecular weight distribution and the nature of end groups.

[a] School of Materials Science and Engineering, Nanyang Technological University, 50 Nanyang Avenue, Singapore 639798. E-mail: YMLam@ntu.edu.sg
[b] Interdisciplinary Graduate School, Nanyang Technological University, Singapore
[c] Energy Research Institute at NTU (ERI@N), Nanyang Technological University, Singapore
[d] School of Physical and Mathematical Sciences, Nanyang Technological University, Singapore

† Electronic supplementary information (ESI) available. See DOI: 10.1039/c6tc02089e

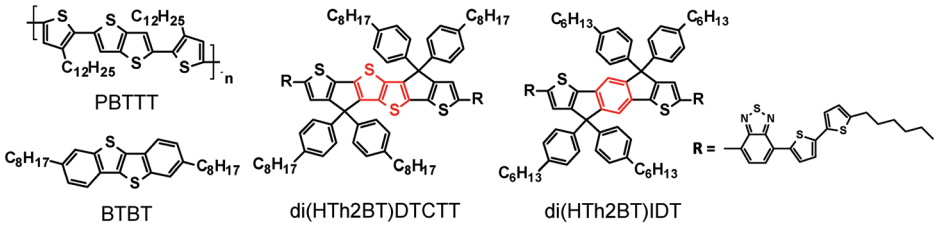

Fig. 1 Chemical structure of PBTTT, BTBT, di(HTh2BT)DTCTT and di(HTh2BT)IDT.

Dithienocyclopenta-thieno[3,2-*b*]thiophene (DTCTT) has a similar structure to IDT except that the central benzene is replaced by a thieno[3,2-*b*]thiophene unit (TT) (Fig. 1). The incorporation of TT units into organic semiconductors has proven to be beneficial for the improvement of charge transport properties due to the high molecular orbital overlap, promoted by the presence of the sulfur atoms. This incorporation has led to some high mobility organic semiconductors such as benzothieno[3,2-*b*]benzothiophene (BTBT) and poly(2,5-bis(3-alkylthiophen-2-yl)thieno[3,2-*b*]thiophenes) (PBTTT).[27–30] Polymers based on DTCTT coupled with several acceptor units have also been reported for OFET and PSC applications with the highest mobilities and PCEs being 5.3×10^{-2} cm^2 V^{-1} s^{-1} and 2.59% for the copolymers benzo[2,1,3]thiadiazole and thieno[3,4-*c*]pyrrole-4,6-dione respectively.[31–33] The ability to absorb light efficiently over a wide spectral range and a strong electron donating ability as well as the rigid backbone structure is especially advantageous for organic dyes used in dye sensitized solar cells and hence high efficiencies of up to 8.9% have been obtained using these dyes such as C243 dye.[34,35] However, no DTCTT based donor molecule for sm-OPV has yet been reported.

Here, we report the first small molecular donor material for sm-OPV incorporating DTCTT units and compare their properties with the IDT-based analogue. It is especially interesting to compare the effect of incorporating a thienothiophene unit in place of benzene in the molecular structure. We expected this modification would improve the hole mobility of the film, leading to a better OPV performance in device. Also, the structural analysis of the molecular form would provide more reliable evidence for the elucidation of the relationship between a certain molecular structure and the device performance than the polymer form does. The structure is based on the conventional D_1–A–D_2–A–D_1 design with DTCTT as the central donor unit, BT units as the acceptors, and bithiophenes as terminal donor moieties. Octylphenyl rings were introduced onto the sp^3 carbon of the cyclopentadienes within the DTCTT unit, to simultaneously suppress the strong π–π stacking and increase the solubility. Such aryl substituents will also increase the photostability of the unit as has been demonstrated in bridged phenylene units in OLED materials.[36]

In this paper, we will discuss how the thienothiophene unit in a molecule based on DTCTT affects its optoelectronic properties and the device performance. A comparison will be made with the IDT analogue that contains a benzene unit.

Experimental

Material

Dibromoindacenodithiophene and 2,5-bis(trimethylstannyl)-thieno[3,2-*b*]thiophene were purchased from SunaTech Inc. 4-*N*-Octyl-bromobenzene was purchased from TCI Inc. Other intermediates were prepared according to literature procedures.[31,32] All reagents purchased commercially were used as received without further purification.

Materials characterization

The ^{1}H and ^{13}C NMR data (400 and 100 MHz, respectively) were obtained using an AVANCE I (Bruker) spectrometer with chemical shifts recorded in $CDCl_3$ solution with TMS as the internal standard. Matrix-assisted laser desorption/ionization time-of-flight (MALDI-TOF) mass spectra were obtained using a Biotech AXIMA-TOF2 (Shimadzu) mass spectrometer. Elemental analysis was performed using a Vario Micro Cube (Elementar) CHNS Analyzer. The UV-Vis absorption spectra were recorded using a UV-2700 spectrophotometer (Shimadzu). Cyclic voltammetry was performed using an Autolab 302N Potentiostat (Metrohm). All CV measurements were recorded in degassed dichloromethane with 0.1 M tetrabutylammonium hexafluorophosphate as the supporting electrolyte (scan rate of 50 mV s^{-1}), using a conventional three electrode configuration consisting of a carbon working electrode, a gold counter electrode, and an Ag/AgCl reference electrode in 3 M KCl(aq). A ferrocene/ferrocenium (Fc/Fc^+) redox couple was also taken as the reference standard. Differential scanning calorimetry (DSC) was performed using DSC Q10 (TA Instruments) under a nitrogen flow (scanning rate of 10 °C min^{-1}).

Device fabrication

Solar cell devices were fabricated using the following steps. After the ITO-coated glass substrates were sequentially cleaned by ultrasonication for 15 min in Hellmanex solution, acetone and isopropyl alcohol, they were plasma-cleaned for 15 min using a Novascan plasma cleaner. Then, PEDOT:PSS (Clevios P Al 4083, filtered at 0.45 μm PVDF) was spin-coated onto the cleaned ITO substrates at 3000 rpm for 60 s to obtain a *ca.* 30 nm thick layer. After transferring the substrates into the glovebox containing a N_2 atmosphere, they were annealed at 140 °C for 10 min. The active layer was prepared by dissolving the donor material and $PC_{71}BM$ (Nano-C) (1 : 3 wt/wt ratio, 15 mg mL^{-1} in an anhydrous chloroform : oDCB = 9 : 1 mixed solution, filtered at 0.20 μm PTFE), followed by spin-coating

onto the PEDOT:PSS on ITO at 1500 rpm for 90 s, resulting in a film of *ca.* 100 nm thickness as determined using a surface analyzer. 0.2 mg mL^{-1} PDMS in chloroform solution was used instead of pure chloroform in the case of the PDMS treated film. After drying inside a glovebox for 1 h, the TiO_x solution was spin-coated on the active layer at 2000 rpm for 60 s, and then subjected to oxidization for 40 min in air. An Al electrode (*ca.* 100 nm) was thermally evaporated at low pressure ($<1 \times 10^{-6}$ Torr) and the complete device with an active area of 0.07 cm^2 was obtained.

Device and thin-film characterization

Current density–voltage (*J–V*) curves were measured inside the glovebox under simulated AM 1.5G illumination (100 mW cm^{-2}) using a Keithley SMU 2612 sourcemeter. The incident-photon-to-current (IPCE) measurement was performed using a Merlin radiometer (Newport) with a monochromator-calibrated wavelength control. A calibrated Si photodiode (Hamamatsu) was used as the reference device for counting the incident photons. AFM images were obtained using Cypher S (Asylum Research). The thin film X-ray diffraction (XRD) pattern was recorded using a D8 Advance (Bruker).

Results and discussion

Synthesis

The synthesis of the novel donor molecule is outlined in Scheme 1. The Stille coupling of 4,8-dibromobenzo[2,1,3]-thiadiazole and 5-tributylstannyl-5′-hexyl-2,2′-bithiophene produced the intermediate **1**. Initially, we tried to couple this bromo compound with distannylated-IDT by the Stille coupling reaction, but the reaction yield was less than 15%, even after refluxing for more than a day, and protonated IDT compounds were detected in the product mixture. It has been reported that protonation resulting from a metal–halogen exchange reaction can take place during metal catalyzed coupling reactions of thiophenes stannylated at the alpha position.[37] Indeed, distannyl-IDT is very sensitive in acidic media, such as chloroform, which produce partially protonated compounds. To promote this Stille coupling, microwave irradiation might be able to help to complete the reaction before protonation can occur but with no guarantee of success as the exchange reaction might also be accelerated by the microwaves.[38] Instead, Suzuki coupling between dibromo-IDT and compound **2** was carried out. The bromo group compound **2** was transformed to a pinacol boronate by the Suzuki–Miyaura borylation reaction. This reaction was almost complete within 1 h and we obtained a dark purple powder of di(HTh2BT)IDT with good yield (52%).

Synthesis of the DTCTT core was performed using a published procedure.[31,32] In this synthesis, di(trimethylstannyl)-thienothiophene was coupled with 2-bromo-3-thiophene carboxylate to obtain precursor **3**. Four octylbenzenes were introduced by reacting **3** with freshly prepared 4-octyl-phenyl magnesium bromide to obtain precursor **4**. Cyclization was performed using an acidic Amberlyst catalyst but the product was found to be unstable and so it was immediately brominated to give dibromo-DTCTT with a reaction yield of 33% for the 2 steps. This bright yellow powder was stable when stored at 5 °C. Di(HTh2BT)DTCTT was synthesized using the same procedure as that for di(Th2BT)IDT and a dark greenish powder was collected with a reaction yield of 50%.

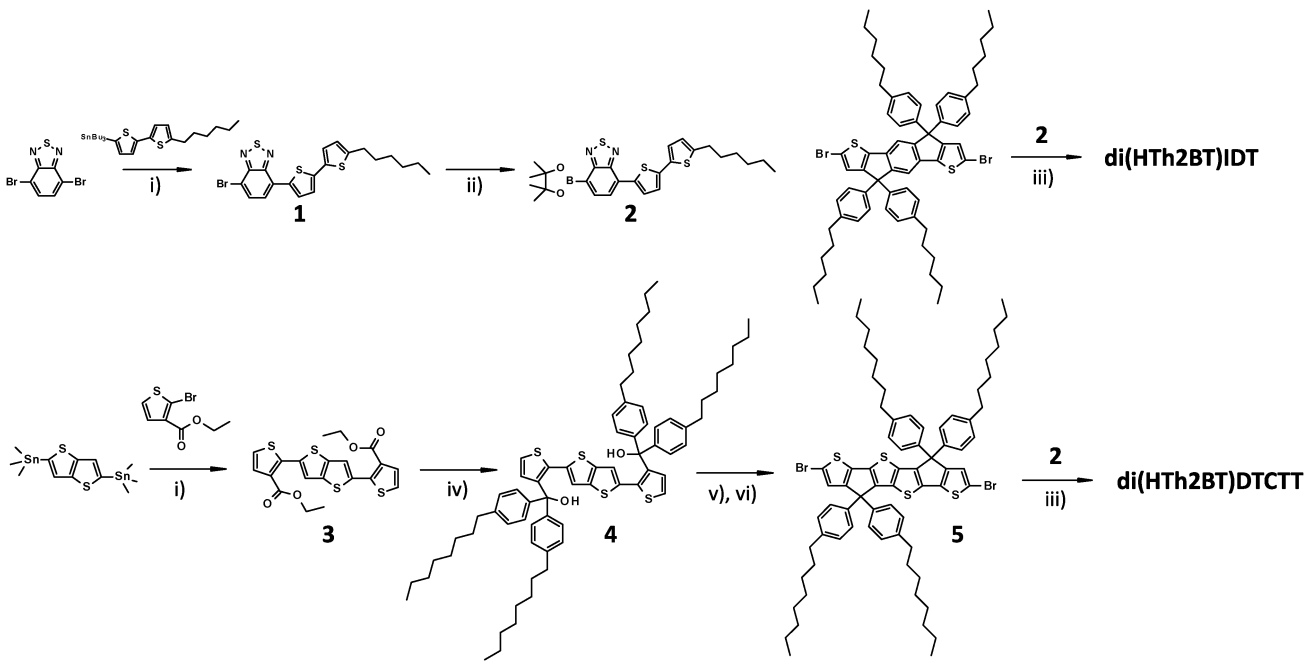

Scheme 1 Synthesis of di(HTh2BT)IDT and di(HTh2BT)DTCTT (i) $Pd(PPh_3)_4$, toluene (ii) B2pin2, $Pd(dppf)Cl_2$, KOAc, toluene (iii) $Pd(PPh_3)_4$, K_2CO_3, THF (iv) OctPhMgBr, THF (v) Amberlyst, toluene (vi) NBS, chloroform.

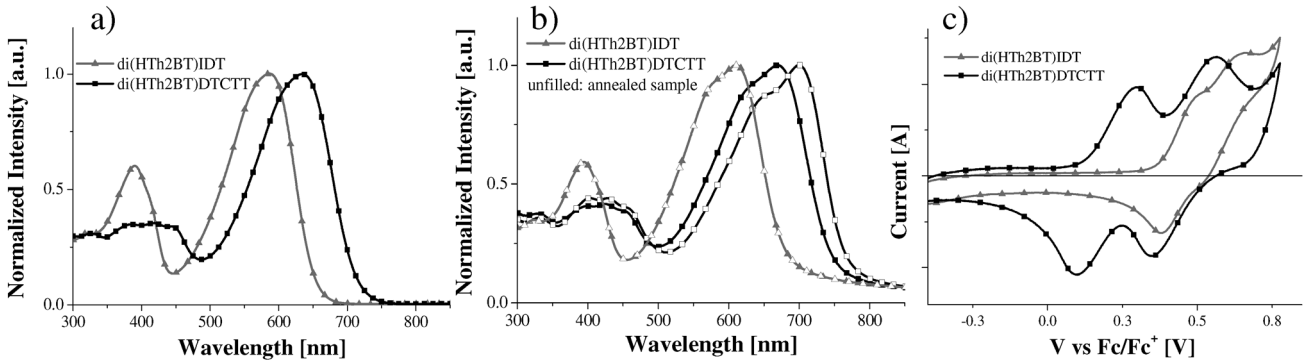

Fig. 2 UV-Vis absorption spectra (a) in chloroform and (b) in film (unfilled symbol: annealed film), and (c) cyclic voltammogram in dichloromethane (grey triangle: IDT black square: DTCTT). Film was prepared by spincoating from chloroform solution.

Optical and electrochemical properties

The absorption spectra were recorded of dilute chloroform solutions and of films spin-cast from chloroform solution (Fig. 2a and b). The cyclic voltammetry was performed in dichloromethane solution under a nitrogen atmosphere to examine the electrochemical properties (Fig. 2c). The parameters obtained are summarized in Table 1.

Di(HTh2BT)IDT can harvest light over a wide range of the visible spectrum. The λ_{max} is 586 nm for the solution and 611 nm for thin films which match well with the reported values.[11] By comparison, the thienothiophene analogue DTCTT showed red-shifted spectra with absorption maxima of 634 nm and 670 nm, respectively. The absorption coefficient calculated by solution spectra is also higher (10.7×10^4) than that of the IDT (8.4×10^4), indicating that thienothiophene enhances the absorptivity. A clear difference was observed in the behavior of annealed films in that no spectral changes were seen for a film of the IDT molecule whereas the absorption maximum of the annealed DTCTT film was red-shifted by 29 nm to 699 nm. These data correspond well with the differential scanning calorimetry (DSC) data which will be discussed later. Both the absorption and DSC data confirmed that the thienothiophene moiety significantly affected the crystallinity due to better π–π stacking resulting in the formation of aggregates. The bandgap calculated from the absorption onset in the unannealed thin film was 1.83 eV for the IDT and 1.66 eV for the DTCTT, which indicated that both compounds were suitable for high efficiency solar cells.

The HOMO/LUMO level was estimated by the optical absorption data and the oxidization peak on cyclic voltammogram. A ferrocene/ferrocenium (Fc/Fc^+) redox couple was used as an internal reference with an absolute redox potential of 4.8 eV below the vacuum level. The HOMO level of the DTCTT was estimated to be −4.95 eV, which is *ca.* 0.2 eV higher than that of IDT: −5.18 eV, while the LUMO levels appeared to be the same. DFT calculations (Fig. S1, ESI†) revealed that the HOMO is distributed all over the conjugated system whereas the LUMO level is localized on the BT moiety to a certain degree, indicating the HOMO is affected by the strong electron-donating ability of the thienothiophene core whereas the LUMO level is mainly determined by the BT moiety.

Crystallization behaviour

Thermal properties of the molecules were analyzed using DSC (Fig. 3) and TGA (Fig. S2, ESI†); the temperatures for the various transitions and decomposition are summarized in Table 2. Di(HTh2BT)IDT showed a melting peak at 115 °C in the first heating cycle and a glass transition at 71 °C in the cooling cycle. In the second heating cycle, no melting peak was observed. Thus, it formed a glass-super cooling phase in the solid state, indicating an amorphous nature of the IDT. Di(HTh2BT)DTCTT showed a melting peak at 235 °C in the first heating cycle and this is much higher than that observed for IDT. Besides the melting peak and a crystallization peak at around 230 °C, weaker peaks were observed upon cooling and upon second heating. Based on the images obtained under a polarized optical microscope (Fig. S3, ESI†), we concluded that these originate from solid-to-solid phase transitions. It is worth noting that these phase transitions were reversible and changing the scanning speed from 10 °C to 1 °C min^{-1} did not change this behavior. Investigation of the polymorphic structure gives insight into the self-assembly structure and the associated intermolecular interaction. Detailed structural analysis is now being carried out. To our surprise, the incorporation of

Table 1 Optical and electrochemical properties of di(Th2BT)IDT and di(HTh2BT)DTCTT

	λ_{max} solution [nm]	ε [M^{-1} cm^{-1}]	λ_{max} film [nm]	λ_{on} [nm]	E_g[a] [eV]	E_{ox} [V *vs.* Fc/Fc^+]	HOMO[b] [eV]	LUMO[c] [eV]
di(Th2BT)IDT	586	8.38×10^4	611 (611)[d]	677 (677)[d]	1.83 (1.83)[d]	0.375	−5.18	−3.35
di(Th2BT)DTCTT	634	10.7×10^4	670 (699)[d]	747 (766)[d]	1.66 (1.62)[d]	0.15	−4.95	−3.29

[a] Calculated by onset wavelength in film state. [b] Estimated by oxidization potential. [c] Calculated by LUMO = HOMO + E_g. [d] Data obtained from annealed sample (100 °C for IDT and 130 °C for DTCTT sample).

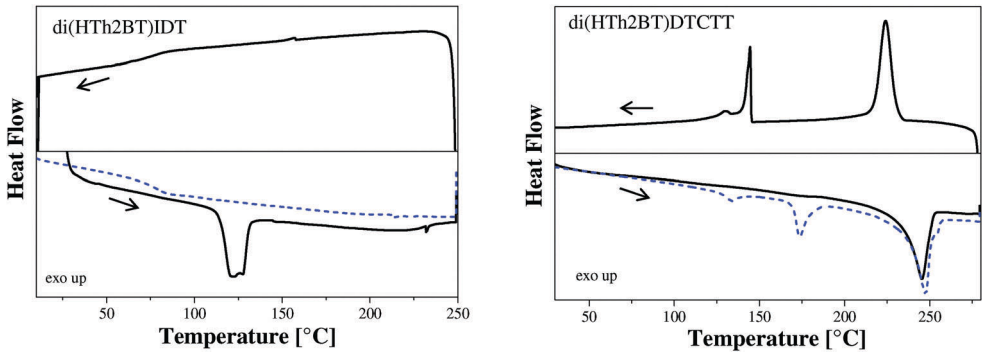

Fig. 3 Differential scanning calorimetry (DSC) of di(HTh2BT)IDT (left) and di(HTh2BT)DTCTT (right); dotted blue line is the 2nd heating cycle.

Table 2 Thermal properties of Th2BT-IDT and Th2BT-DTCTT

	1st heating °C [kJ mol^{-1}]	Cooling °C [kJ mol^{-1}]	2nd heating °C [kJ mol^{-1}]	T_{dcmp} [°C]
di(HTh2BT)IDT	T_m: 114.9 [18.2]	T_g: 70.8	T_g: 79.0	430[a]
di(HTh2BT)DTCTT	T_m: 234.9 [43.3]	T_{cr}: 230.3 [39.4]	T_{tr1}: 127.6 [2.60]	420[b]
			T_{tr2}: 169.8 [12.3]	
		T_{tr}: 145.2 [18.3]	T_m: 237.3 [44.7]	

T_{dcmp}: decomposition temperature, T_m: melting temperature, T_g: glass transition temperature, T_{cr}: crystallization temperature, T_{tr}: phase transition temperature. [a] Taken from ref. 11. [b] Measured from TGA under nitrogen atmosphere.

the thienothiophene moiety, compared to the case of benzene, completely changed the self-organization character of the molecules from amorphous to crystalline even in the presence of bulky phenyl groups on the sp^3 carbon. Both compounds have decomposition temperatures of over 400 °C, implying that they are stable under the PV operating conditions.

Hole-only devices with the configuration of ITO/PEDOT:PSS/pristine film/Au were fabricated and the dark current was measured to estimate the hole mobility of the thin film. The square root of the dark current in the saturated current region under high bias voltage was found to vary proportionally to V (Fig. S4, ESI†). This indicates the operation condition of space-charge-limited-current (SCLC). The hole mobility μ_0 at zero field was obtained by fitting the experimental dark current to the SCLC model equation.

$$J = \frac{9}{8}\varepsilon_0\varepsilon_r\mu_0 \exp\left(0.89\beta\sqrt{\frac{V - V_{bi}}{L}}\right)\frac{(V - V_{bi})^2}{L^3} \quad (1)$$

Given that the dielectric constant of the material, ε_r, is 3 (assumed from the typical value of organic semiconductors), the hole mobility of the DTCTT and the IDT pristine film are estimated to be 1.6×10^{-3} and 7.3×10^{-5} cm^2 V^{-1} s^{-1} respectively. The hole mobility of the DTCTT is one order of magnitude higher than that of the IDT. This is consistent with the higher degree of order in the crystalline DTCTT film compared to the amorphous IDT film.

These improvements in solid-state organization with the incorporation of the thienothiophene moiety have a strong implication for PV applications as they can potentially lead to stronger absorption and also better charge transport.

Photovoltaic performance and thin film morphology

Both compounds were blended with $PC_{71}BM$ and incorporated into bulk heterojunction solar cell devices with the following device structure: ITO/PEDOT:PSS/active layer/TiO_x/Al. In this device architecture, TiO_x interlayer[39] was included as an electron transporting interlayer. The optimum current density *vs.* voltage (*J*–*V*) curves with a donor–acceptor ratio of 1 : 3 (wt/wt) are shown in Fig. 4 and the parameters are presented in Table 3. The IDT based solar cell with a 1 : 3 donor–acceptor ratio was also prepared according to the published literature[11] and we obtained very similar values to the previously reported J_{sc} values of −9.3 mA cm^{-2} and V_{oc} of 0.94 V, respectively with a PCE of 3.2%. As for the DTCTT devices, a range of donor–acceptor ratios from 1 : 1 to 1 : 4 (wt/wt) was investigated. At large donor ratios, the device performance was poor (at 1 : 1 ratio, PCE of 0.72% with J_{sc} of −2.8 mA cm^{-2}, V_{oc} of 0.73 and FF of 0.34). The best result was obtained for the donor–acceptor ratio of 1 : 3 – PCE of 2.6% with a J_{sc} of −8.8 mA cm^{-2}, V_{oc} of 0.74 and FF of 0.41. Compared to the reported DTCTT-BT copolymer mentioned earlier in the introduction, comparable J_{sc} is obtained but the V_{oc} is increased by 0.15 V (V_{oc} of 0.59 V) for DTCTT with hexyl phenyl side groups and 0.1 V (V_{oc} of 0.64 V) for DTCTT with octyloxy phenyl side groups.[31,32] There is a general trend for small molecular donors for showing a higher V_{oc} value than the analogous polymer.[40,41] Further optimization carried out by annealing at various temperatures and using DIO additive did not result in better performance. PDMS was used to modify the viscosity of solution for the purpose of improving the film quality[42] and a slight improvement was obtained: a PCE of 2.8% with J_{sc} of −9.33 mA cm^{-2}, V_{oc} of 0.73, and FF of 0.42. Compared to the IDT molecule, the J_{sc} is of comparable value but the V_{oc} is lower by 0.2 V,

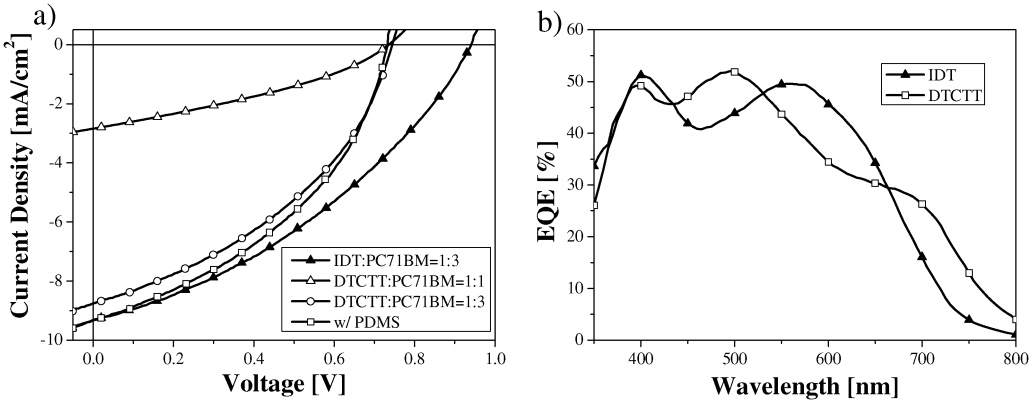

Fig. 4 (a) Current density–voltage characteristics of each device in a structure of ITO/PEDOT:PSS/active layer/TiO_x/Al under the illumination of AM1.5G, 100 mW cm^{-2}. (b) EQE curves of the devices based on di(HTh2BT)IDT : $PC_{71}BM$ = 1 : 3 and di(HTh2BT)DTCTT : $PC_{71}BM$ = 1 : 3 with PDMS treatment.

Table 3 Photovoltaic performance of the bulk heterojunction molecular donor/$PC_{71}BM$ devices[a]

Active layer	D/A ratio	PCE [%]	J_{sc} [mA cm^{-2}]	V_{oc} [V]	FF
IDT : $PC_{71}BM$	1 : 3	3.21 (3.00 ± 0.11)	−9.32 (−8.94 ± 0.25)	0.94 (0.94 ± 0.00)	0.37 (0.36 ± 0.01)
DTCTT : $PC_{71}BM$	1 : 1	0.72 (0.68 ± 0.02)	−2.84 (−2.67 ± 0.07)	0.73 (0.73 ± 0.01)	0.34 (0.35 ± 0.00)
DTCTT : $PC_{71}BM$	1 : 3	2.63 (2.48 ± 0.12)	−8.76 (−8.53 ± 0.20)	0.74 (0.74 ± 0.00)	0.41 (0.39 ± 0.01)
w/PDMS	1 : 3	2.84 (2.67 ± 0.08)	−9.33 (−8.85 ± 0.22)	0.73 (0.73 ± 0.00)	0.42 (0.41 ± 0.00)

[a] Average values inside parenthesis were calculated from 8 devices.

corresponding to the difference in the HOMO levels estimated by cyclic voltammetry. A low FF is the main cause for the rather low PCE value.

To investigate the causes of this low FF, XRD and AFM studies were performed on thin films. The sample crystallinity in film state was measured using XRD (Fig. S5, ESI†). The DTCTT pristine film showed a strong diffraction peak at $2\theta = 3.65^\circ$, whereas the IDT pristine film showed no peak due to its amorphous nature. This is a direct evidence for induced crystallinity due to the incorporation of thienothiophene into the core structure. Annealing at 200 °C induced relaxation of the aggregation structure and two peaks at $2\theta = 4.04$ and 8.12° appeared, indicating a lamellar structure ($d = 2.2$ nm). However, no peak was observed in the blend film with $PC_{71}BM$ for both 1 : 1 and 1 : 3 wt ratios. It seems that $PC_{71}BM$ prevents the effective aggregation of the DTCTT. The lack of strong crystallinity in the blend film is thus believed to be the reason for the low fill factor as a high mobility value ($>10^4$ cm^2 V^{-1} s^{-1}) as well as balanced hole and electron transport properties are necessary to achieve a high fill factor.[43]

The surface morphology of the DTCTT in the film state was analyzed using AFM (Fig. 5). Sample films were prepared by spin-coating on top of a PEDOT:PSS layer with the same deposition conditions as those used for the solar cell fabrication. As shown on the height image and phase image, the difference in donor–acceptor weight ratio can result in a large morphological variation. It seems that DTCTT tends to form a rough surface as can be seen on the pristine film (RMS roughness factor of 14.2 nm). The blend film with $PC_{71}BM$ makes it smoother (2.38 nm for 1 : 1 ratio) and finally a very smooth film (0.67 nm for 1 : 3 ratio) was obtained at the optimum donor–acceptor ratio. Many pores were observed in the blend film at 1 : 1 ratio. This rough morphology eventually leads to the direct contact between the cathode and anode interlayer which may explain the large leakage current measured in the device with this blend ratio. The good film morphology for 1 : 3 D–A ratio film resulted in the best device performance with a high J_{sc} of about −9.0 mA cm^{-2}. The well-mixed morphology of donor and acceptor induces good exciton separation; the very smooth surface morphology also leads to enhanced charge extraction toward electrodes.

Finally, the EQE spectra of complete devices were compared between the IDT and the DTCTT based devices (Fig. 4 right). For the DTCTT sample, PDMS additive was used in active layer preparation. The calculated J_{sc} from the EQE spectra and the experimental data matched within a 5% range. Both the IDT and the DTCTT showed an EQE response over a broad range of wavelengths from 350 nm to 800 nm and this agrees very well with the UV-Vis absorption data. Red-shifted absorption profile of the DTCTT especially contributed to the higher EQE response over 670 nm. However, the EQE spectrum indicates that the photogeneration takes place mainly from $PC_{71}BM$ exciton. This can be simply explained by the UV-Vis absorption spectra of the blend films (Fig. S6, ESI†). The absorption spectrum of the 1 : 3 blend film matches well with the EQE response, indicating that the amount of DTCTT in film was not optimal. The 1 : 1 blend film has a balanced absorption spectrum contributed by both the $PC_{71}BM$ and the DTCTT, but the film quality was poor as was seen on the AFM image. Further structural modification is necessary to promote an effective crystallization and uniform film morphology.

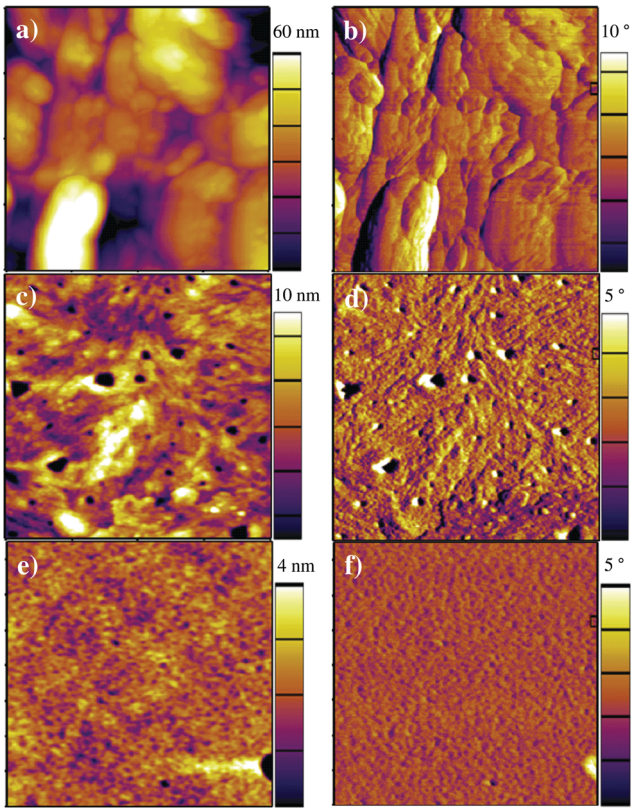

Fig. 5 AFM (2 × 2 μm) height and phase image of di(HTh2BT)DTCTT pristine film (a and b), blend film with $PC_{71}BM$ (1 : 1 wt/wt) (c and d), and (1 : 3 wt/wt) (e and f).

Conclusion

We have reported a novel molecular donor material with DTCTT as the central building block, and systematically compared it with the analogous IDT based material. Although the only structural difference is the incorporation of thienothiophene and benzene units, respectively, in the core structure, clear differences were observed in their structural, optical, electrochemical, thermal properties, and OPV device performance. The electron-rich TT core induced a red-shift in the absorption and a higher HOMO level. Furthermore, this new molecular donor material has higher thermal stability compared to IDT based materials and the new molecular structure promoted better crystallinity, possibly because of the strong S–S intermolecular interactions which produce a greater overlap of frontier molecular orbitals. In OPV device performance, larger J_{sc} was expected based on the light absorption profile and the J_{sc} obtained was indeed a high value of -9.33 mA cm^{-2}. However that was only comparable to the IDT based devices because of the rough surface film and the lack of effective crystallization. A rather low PCE of 2.84% was obtained in the devices. Increasing the low FF of 0.42 will be the key factor to contribute to the further development of these DTCTT based molecular donor materials. This could be achieved by modifying the molecular structure to promote effective crystallization either by extending aromatic linker parts or fixing intramolecular conformation between DTCTT core and BT units. This modification work is ongoing. Overall, enhanced crystallinity of the DTCTT is a promising feature as other efficient IDT-based OPV material improved their crystallinity by extending conjugation,[13] replacing bulky phenyls on the sp^3 carbon to flexible alkyl chains,[14] and extending the IDT backbone itself.[44,45] The results presented in this paper provide suggestions for the further development of DTCTT based functional materials.

References

1 W. Zhang, J. Smith, S. E. Watkins, R. Gysel, M. McGehee, A. Salleo, J. Kirkpatrick, S. Ashraf, T. Anthopoulos, M. Heeney and I. McCulloch, *J. Am. Chem. Soc.*, 2010, **132**, 11437–11439.
2 I. McCulloch, R. S. Ashraf, L. Biniek, H. Bronstein, C. Combe, J. E. Donaghey, D. I. James, C. B. Nielsen, B. C. Schroeder and W. Zhang, *Acc. Chem. Res.*, 2012, **45**, 714–722.
3 X. Zhang, H. Bronstein, A. J. Kronemeijer, J. Smith, Y. Kim, R. J. Kline, L. J. Richter, T. D. Anthopoulos, H. Sirringhaus, K. Song, M. Heeney, W. Zhang, I. McCulloch and D. M. DeLongchamp, *Nat. Commun.*, 2013, **4**, 2238.
4 X. Guo, M. Zhang, J. Tan, S. Zhang, L. Huo, W. Hu, Y. Li and J. Hou, *Adv. Mater.*, 2012, **24**, 6536–6541.
5 D. Dang, W. Chen, S. Himmelberger, Q. Tao, A. Lundin, R. Yang, W. Zhu, A. Salleo, C. Müller and E. Wang, *Adv. Energy Mater.*, 2014, **4**, 1400680.
6 D. B. Sulas, K. Yao, J. J. Intemann, S. T. Williams, C.-Z. Li, C.-C. Chueh, J. J. Richards, Y. Xi, L. D. Pozzo, C. W. Schlenker, A. K. Y. Jen and D. S. Ginger, *Chem. Mater.*, 2015, **27**, 6583–6591.
7 Y.-C. Chen, C.-Y. Yu, Y.-L. Fan, L.-I. Hung, C.-P. Chen and C. Ting, *Chem. Commun.*, 2010, **46**, 6503–6505.
8 Y. Sun, G. C. Welch, W. L. Leong, C. J. Takacs, G. C. Bazan and A. J. Heeger, *Nat. Mater.*, 2012, **11**, 44–48.
9 Z. B. Henson, K. Mullen and G. C. Bazan, *Nat. Chem.*, 2012, **4**, 699–704.
10 Y. Chen, X. Wan and G. Long, *Acc. Chem. Res.*, 2013, **46**, 2645–2655.
11 W. Yong, M. Zhang, X. Xin, Z. Li, Y. Wu, X. Guo, Z. Yang and J. Hou, *J. Mater. Chem. A*, 2013, **1**, 14214.
12 D. Liu, M. Xiao, Z. Du, Y. Yan, L. Han, V. A. L. Roy, M. Sun, W. Zhu, C. S. Lee and R. Yang, *J. Mater. Chem. C*, 2014, **2**, 7523–7530.
13 X. Liu, Q. Li, Y. Li, X. Gong, S.-J. Su and Y. Cao, *J. Mater. Chem. A*, 2014, **2**, 4004.
14 J.-L. Wang, Q.-R. Yin, J.-S. Miao, Z. Wu, Z.-F. Chang, Y. Cao, R.-B. Zhang, J.-Y. Wang, H.-B. Wu and Y. Cao, *Adv. Funct. Mater.*, 2015, **25**, 3514–3523.
15 H. Bai, P. Cheng, Y. Wang, L. Ma, Y. Li, D. Zhu and X. Zhan, *J. Mater. Chem. A*, 2014, **2**, 778–784.
16 Y. Lin, J. Wang, Z. G. Zhang, H. Bai, Y. Li, D. Zhu and X. Zhan, *Adv. Mater.*, 2015, **27**, 1170–1174.
17 Y. Lin, Q. He, F. Zhao, L. Huo, J. Mai, X. Lu, C. J. Su, T. Li, J. Wang, J. Zhu, Y. Sun, C. Wang and X. Zhan, *J. Am. Chem. Soc.*, 2016, **138**, 2973–2976.
18 W. Zhao, D. Qian, S. Zhang, S. Li, O. Inganäs, F. Gao and J. Hou, *Adv. Mater.*, 2016, **28**, 4734–4739.

19 J.-S. Wu, S.-W. Cheng, Y.-J. Cheng and C.-S. Hsu, *Chem. Soc. Rev.*, 2015, **44**, 1113–1154.
20 K. Takimiya, S. Shinamura, I. Osaka and E. Miyazaki, *Adv. Mater.*, 2011, **23**, 4347–4370.
21 W. Ni, M. Li, F. Liu, X. Wan, H. Feng, B. Kan, Q. Zhang, H. Zhang and Y. Chen, *Chem. Mater.*, 2015, **27**, 6077–6084.
22 J. A. Love, I. Nagao, Y. Huang, M. Kuik, V. Gupta, C. J. Takacs, J. E. Coughlin, L. Qi, T. S. van der Poll, E. J. Kramer, A. J. Heeger, T. Q. Nguyen and G. C. Bazan, *J. Am. Chem. Soc.*, 2014, **136**, 3597–3606.
23 X. Zhu, B. Xia, K. Lu, H. Li, R. Zhou, J. Zhang, Y. Zhang, Z. Shuai and Z. Wei, *Chem. Mater.*, 2016, **28**, 943–950.
24 J. Wolf, M. Babics, K. Wang, Q. Saleem, R.-Z. Liang, M. R. Hansen and P. M. Beaujuge, *Chem. Mater.*, 2016, **28**, 2058–2066.
25 L. Liang, J.-T. Wang, X. Xiang, J. Ling, F.-G. Zhao and W.-S. Li, *J. Mater. Chem. A*, 2014, **2**, 15396–15405.
26 W. Li, W. Deng, K. Wu, G. Xie, C. Yang, H. Wu and Y. Cao, *J. Mater. Chem. C*, 2016, **4**, 1972–1978.
27 J. I. Park, J. W. Chung, J. Y. Kim, J. Lee, J. Y. Jung, B. Koo, B. L. Lee, S. W. Lee, Y. W. Jin and S. Y. Lee, *J. Am. Chem. Soc.*, 2015, **137**, 12175–12178.
28 H. Iino, T. Usui and J. Hanna, *Nat. Commun.*, 2015, **6**, 6828.
29 M. O. Ahmed, C. Wang, P. Keg, W. Pisula, Y.-M. Lam, B. S. Ong, S.-C. Ng, Z.-K. Chen and S. G. Mhaisalkar, *J. Mater. Chem.*, 2009, **19**, 3449.
30 I. McCulloch, M. Heeney, C. Bailey, K. Genevicius, I. MacDonald, M. Shkunov, D. Sparrowe, S. Tierney, R. Wagner, W. Zhang, M. L. Chabinyc, R. J. Kline, M. D. McGehee and M. F. Toney, *Nat. Mater.*, 2006, **5**, 328–333.
31 H. Bronstein, R. S. Ashraf, Y. Kim, A. J. White, T. Anthopoulos, K. Song, D. James, W. Zhang and I. McCulloch, *Macromol. Rapid Commun.*, 2011, **32**, 1664–1668.
32 Y. J. Cheng, C. H. Chen, T. Y. Lin and C. S. Hsu, *Chem. – Asian J.*, 2012, **7**, 818–825.
33 B. C. Schroeder, R. S. Ashraf, S. Thomas, A. J. White, L. Biniek, C. B. Nielsen, W. Zhang, Z. Huang, P. S. Tuladhar, S. E. Watkins, T. D. Anthopoulos, J. R. Durrant and I. McCulloch, *Chem. Commun.*, 2012, **48**, 7699–7701.
34 N. Cai, R. Li, Y. Wang, M. Zhang and P. Wang, *Energy Environ. Sci.*, 2013, **6**, 139–147.
35 H. Li, T. M. Koh, Y. Hao, F. Zhou, Y. Abe, H. Su, A. Hagfeldt and A. C. Grimsdale, *ChemSusChem*, 2014, **7**, 3396–3406.
36 A. C. Grimsdale, K. Leok Chan, R. E. Martin, P. G. Jokisz and A. B. Holmes, *Chem. Rev.*, 2009, **109**, 897–1091.
37 A. Pelter, I. Jenkins and D. E. Jones, *Tetrahedron*, 1997, **53**, 10357–10400.
38 T. S. van der Poll, J. A. Love, T. Q. Nguyen and G. C. Bazan, *Adv. Mater.*, 2012, **24**, 3646–3649.
39 J. Y. Kim, S. H. Kim, H. H. Lee, K. Lee, W. Ma, X. Gong and A. J. Heeger, *Adv. Mater.*, 2006, **18**, 572–576.
40 B. Walker, C. Kim and T.-Q. Nguyen, *Chem. Mater.*, 2011, **23**, 470–482.
41 J. Zhou, Y. Zuo, X. Wan, G. Long, Q. Zhang, W. Ni, Y. Liu, Z. Li, G. He, C. Li, B. Kan, M. Li and Y. Chen, *J. Am. Chem. Soc.*, 2013, **135**, 8484–8487.
42 K. R. Graham, J. Mei, R. Stalder, J. W. Shim, H. Cheun, F. Steffy, F. So, B. Kippelen and J. R. Reynolds, *ACS Appl. Mater. Interfaces*, 2011, **3**, 1210–1215.
43 C. M. Proctor, J. A. Love and T.-Q. Nguyen, *Adv. Mater.*, 2014, **26**, 5957–5961.
44 H.-C. Wang, L.-M. Tang, L. Zuo, H. Chen and Y.-X. Xu, *RSC Adv.*, 2015, **5**, 80677–80681.
45 J. J. Intemann, K. Yao, F. Ding, Y. Xu, X. Xin, X. Li and A. K. Y. Jen, *Adv. Funct. Mater.*, 2015, **25**, 4889–4897.